

ERROR ANALYSIS FOR PEPPERPOT EMITTANCE MEASUREMENTS REDUX: CORRELATED PHASE SPACES*

S. Lidia^{#†}, K. Murphy[‡], Lawrence Berkeley National Laboratory, Berkeley, CA, USA

Abstract

Recently, Jolly *et al.* presented an analysis of the rms emittance measurement errors from a first principles approach [1]. Their approach demonstrated the propagation of errors in the single-plane rms emittance determination from several instrument and beam related sources. We have extended the analysis of error propagation and estimation to the fully correlated 4-D phase space emittances obtained from pepperpot measurements. We present the calculation of the variances using a Cholesky decomposition approach. Pepperpot data from recent experiments on the NDCX-II beamline are described, and estimates of the emittances and measurement errors for the 4-D as well as the projected rms emittances in this coupled system are presented.

INTRODUCTION

Jolly, *et al.* [1] recently published an analysis of the data acquisition and uncertainty estimation of beam emittances derived from pepperpot measurements. There, they presented a first principles methodology for propagating measurement errors into the nonlinear functions of position, angle and beamlet intensity that are typically used to calculate the horizontal or vertical root-mean-squared (rms) emittances. Estimates of measurement errors were discussed that stemmed from the practical implementation of the pepperpot measurement system. The dominant sources of measurement error were the spacing of holes in the pepperpot mask; the camera resolution and drift distance between mask and scintillation screen; and beam intensity variation and background intensity noise levels. Additional errors in the measurement system were not included, so that the estimates of uncertainty represent lower limits on the total error.

A pepperpot image and its correlations to the background mask can be utilized to estimate the complete 4-D phase space emittance by analyzing all 10 independent correlation terms in the 4-D beam matrix. In this paper we extend Jolly, *et al.*'s formalism to estimate the uncertainty of the 4-D emittance and related quantities that include the correlations between the horizontal and vertical phase spaces. The results of this analysis can be applied to coupled systems found in solenoidal or skew quadrupole transport lattices, and beams that carry significant canonical angular momentum.

*This work was supported by the Director, Office of Science, Office of Fusion Energy Sciences, of the U.S. Department of Energy under Contract No. DE-AC02-05CH11231.

#lidia@frib.msu.edu

†Presently at Facility for Rare Isotope Beams, Michigan State University.

‡Presently at Department of Physics, University of Chicago.

CORRELATED PHASE SPACES

The 4-D beam covariance matrix is constructed from the density-weighted, rms product averages of the beam distribution,

$$\Sigma_4 = \begin{pmatrix} \langle xx \rangle & \langle xx' \rangle & \langle xy \rangle & \langle xy' \rangle \\ \langle xx' \rangle & \langle x'x' \rangle & \langle x'y \rangle & \langle x'y' \rangle \\ \langle xy \rangle & \langle x'y \rangle & \langle yy \rangle & \langle yy' \rangle \\ \langle xy' \rangle & \langle x'y' \rangle & \langle yy' \rangle & \langle y'y' \rangle \end{pmatrix} \quad (1)$$

Here, the individual product terms are defined by

$$\langle fg \rangle = \frac{\sum_i \rho_i f_i g_i}{\sum_i \rho_i}, \quad (2)$$

where the index i labels the coordinates in the 4-D space of $\{x, x', y, y'\}$ and ρ is the local beam density in that space. We assume that the 10 unique terms are linearly-independent of each other.

The 4-D beam matrix can be expressed in the symmetric, block form that reveals the separate, Cartesian sub-spaces as well as the correlation between them,

$$\Sigma_4 = \begin{pmatrix} \Sigma_x & C \\ C^T & \Sigma_y \end{pmatrix}. \quad (3)$$

We note that other representations [2,3] are also used.

The definitions of rms emittances follow from the determinants of the beam matrix. The determinant and emittance of the 2-D Cartesian (sub-)phase space has the well known definition:

$$\det \Sigma_x = |\Sigma_x| = \langle xx \rangle \langle x'x' \rangle - \langle xx' \rangle^2 = \tilde{\epsilon}_x^2. \quad (4)$$

We carry the definition to the 4-D space and 4-D emittance:

$$\tilde{\epsilon}_4^2 = |\Sigma_4|. \quad (5)$$

To compare the equivalent beam quality defined by the 4-D emittance measure, we define an equivalent 2-D emittance

$$\tilde{\epsilon}_2^2 = |\Sigma_2| = |\Sigma_4|^{1/2}. \quad (6)$$

For transversely uncoupled phase spaces, $\Sigma_4 = \begin{pmatrix} \Sigma_x & 0 \\ 0 & \Sigma_y \end{pmatrix}$, and $|\Sigma_2| = |\Sigma_x| |\Sigma_y|$ so that $\tilde{\epsilon}_2^2 = \tilde{\epsilon}_x \tilde{\epsilon}_y$.

We utilize the equivalent 2-D rms emittance measure, $\tilde{\epsilon}_2$, as a basis of comparison with the single-plane rms

emittances, $\tilde{\epsilon}_x$ and $\tilde{\epsilon}_y$. We will also make use of the following definition of normalized, edge emittances, $\epsilon_a = 4\gamma\beta\tilde{\epsilon}_a$, where $\tilde{\epsilon}_a$ is any of the above mentioned 2-D or single plane rms emittances.

CHOLESKY DECOMPOSITION OF BEAM COVARIANCE MATRIX

The analysis of error propagation from known measurement uncertainties into the 4-D or equivalent 2-D emittance measures can be made more computationally tractable if a matrix factorization is utilized. The Cholesky decomposition [4] is unique for positive-definite, symmetric, square matrices. This factorization produces a product of a lower-diagonal matrix (L) with its transpose, an upper diagonal matrix (L^T). Here, we opt to use a variant of the Cholesky decomposition, $A = LDL^T$, where A is the original matrix, and D is a block diagonal form.

The decomposition of the 4D beam covariance matrix

$$\begin{aligned} \Sigma_4 &= \begin{pmatrix} \Sigma_x & C \\ C^T & \Sigma_y \end{pmatrix} = LDL^T \\ &= \begin{pmatrix} I & 0 \\ S & I \end{pmatrix} \begin{pmatrix} D_1 & 0 \\ 0 & D_2 \end{pmatrix} \begin{pmatrix} I & S^T \\ 0 & I \end{pmatrix} \end{aligned} \quad (7)$$

With this decomposition, $|\Sigma_4| = |D_1||D_2|$. In terms of the Cartesian sub-spaces and correlation matrix C ,

$$D_1 = \Sigma_x, \quad (8)$$

$$D_2 = \Sigma_y - C^T(\Sigma_x^{-1})^T C. \quad (9)$$

This last form has its determinant expressed in terms of the elementary products as

$$\begin{aligned} |D_2| &= \left(\langle yy \rangle - \frac{v_1}{|\Sigma_x|} \right) \left(\langle y'y' \rangle - \frac{v_4}{|\Sigma_x|} \right) - \\ &\left(\langle yy' \rangle - \frac{v_2}{|\Sigma_x|} \right)^2, \end{aligned} \quad (10)$$

where

$$\begin{aligned} v_1 &= \langle xy \rangle^2 \langle x'x' \rangle - 2\langle xy \rangle \langle xx' \rangle \langle x'y \rangle + \langle xx \rangle \langle x'y \rangle^2, \\ v_2 &= \langle xy \rangle \langle x'x' \rangle \langle xy' \rangle - \langle xy \rangle \langle xx' \rangle \langle x'y' \rangle + \langle x'y \rangle \langle xx \rangle \langle x'y' \rangle - \langle x'y \rangle \langle xx' \rangle \langle x'y' \rangle, \\ v_4 &= \langle xy' \rangle^2 \langle x'x' \rangle - 2\langle xy' \rangle \langle xx' \rangle \langle x'y' \rangle + \langle xx \rangle \langle x'y' \rangle^2. \end{aligned} \quad (11)$$

ANALYSIS OF VARIANCE

The calculation of the combined variance proceeds typically [5]. A function, f , with independent variables (x ,

y, z, \dots), has a variance, σ_f^2 , defined by $\sigma_f^2 = \left(\frac{\partial f}{\partial x}\right)^2 \sigma_x^2 + \left(\frac{\partial f}{\partial y}\right)^2 \sigma_y^2 + \left(\frac{\partial f}{\partial z}\right)^2 \sigma_z^2 + \dots$, where the variance in the measurement of the independent variables is given by σ_x^2, σ_y^2 , etc.

We calculate the variance of the 4-D beam matrix determinant, against the set of independent variables: $\langle xx \rangle, \langle x'x' \rangle, \langle xy \rangle, \langle xy' \rangle, \langle x'y \rangle, \langle x'y' \rangle, \langle yy \rangle, \langle yy' \rangle$, and $\langle y'y' \rangle$.

$$\sigma_{|\Sigma_4|}^2 = \sum_{\langle ab \rangle} \left(\frac{\partial |\Sigma_4|}{\partial \langle ab \rangle} \right)^2 \sigma_{\langle ab \rangle}^2, \quad (12)$$

where $\langle ab \rangle$ is a member of the set of 10 linearly-independent products.

The variance of the equivalent 2-D emittance is determined by applying the linear uncertainty estimation to (6)

$$\begin{aligned} \sigma_{\tilde{\epsilon}_2}^2 &= \sum_{\langle ab \rangle} \left(\frac{\partial \tilde{\epsilon}_2}{\partial \langle ab \rangle} \right)^2 \sigma_{\langle ab \rangle}^2 = \\ &\sum_{\langle ab \rangle} \left(\left[\frac{d\tilde{\epsilon}_2}{d|\Sigma_4|} \right] \left[\frac{\partial |\Sigma_4|}{\partial \langle ab \rangle} \right] \right)^2 \sigma_{\langle ab \rangle}^2 = \\ &\sum_{\langle ab \rangle} \left[\frac{1}{4|\Sigma_4|^{3/4}} \right]^2 \left(\left[\frac{\partial |\Sigma_4|}{\partial \langle ab \rangle} \right] \right)^2 \sigma_{\langle ab \rangle}^2 \end{aligned} \quad (13)$$

$$\sigma_{\tilde{\epsilon}_2}^2 = \frac{\sigma_{|\Sigma_4|}^2}{16|\Sigma_4|^{3/2}} \quad (14)$$

NDCX-II PEPPERPOT DESIGN AND MEASUREMENTS

The NDCX-II facility permits user experiments in the warm, dense matter regime, where matter is isochorically heated near solid density to temperatures in the eV range. Ion beams compressed to ns-scale pulse duration and focused with mm-scale spots onto micron-scale thickness targets can accomplish this task of target heating within the characteristic time of hydrodynamic expansion of the target material. The detailed physics design [6] and engineering [7] of the NDCX-II accelerator facility have been previously described. The first stage of beamline commissioning demonstrated the successful tuning of the beam transport lattice and the accelerating waveforms to deliver 30-50 nC, with normalized edge emittance of 1-2 π -mm-mrad, and to compress the pulse duration from ~600 ns at injection to <50 ns (FWHM) at the target plane [8].

The diagnostic end station houses the main complement of intercepting beam diagnostics, depicted in Fig. 1. The full instrumentation package includes a deep Faraday cup (14.2 cm long by 12 cm wide with a 10 cm entrance aperture), a horizontal slit and slit-cup analyzer, a vertical slit and slit-cup analyzer, a pepperpot mask and a 10.16-cm (4-inch) square optical scintillator (100 μ m thick Al_2O_3). A fast gated (~30 ns minimum), image intensified (ICCD) camera (Princeton Instruments PI-MAX II, 16-bit, 512x512 CCD array) is rear-mounted to collect the

fluorescence signal from the scintillator plate. The deep Faraday cup is differentially biased to reject incoming electrons entrained with the ion beam, as well as to collect secondary electrons emitted during the ion current collection. The collector plane of the deep Faraday cup and the front surface of the scintillator coincide with the experimental target plane. Various planar targets may be mounted at the end of the scintillator/Faraday cup paddle. High voltage SHV feedthroughs allow bias potentials to be applied to the Faraday cup and slit cup suppressor and collector electrodes, and to the bias mesh on the upstream face of the optical scintillator. Capacitive dividers allow low amplitude beam-induced signals to be acquired from the high voltage biased electrodes.

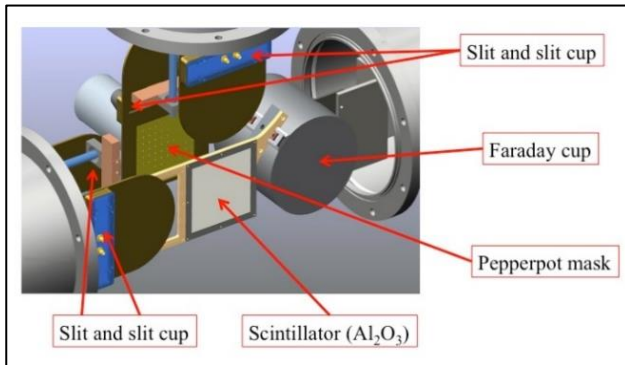


Figure 1: NDCX-II diagnostic end station.

The pepperpot mask (Fig. 2) and associated scintillator diagnostic has been designed and initially optimized to function with the high perveance, ~50-350 keV lithium ions. The mask is fabricated from 12.7 μm 304 stainless steel, and holds a rectangular pattern of 0.254 mm (0.010-inch) diameter holes spaced 3.81 mm (0.150-inch) apart (center-to-center). A scintillator screen is rigidly attached to the pepperpot mask holder, and spaced 17.5 mm downstream from the mask.

Analysis of the pepperpot images is accomplished utilizing a custom Python analysis routine: (i) beam-derived images and background images (resolution 4.7 pixels/mm) are obtained with defined gate windows around the beam current peak; (ii) background images are subtracted from beam-generated images; (iii) a Sobel filter [9] is applied to further assist in discriminating peaks from background; (iv) the images peaks are mapped to the known grid pattern to generate spatially correlated offsets and construct the 4-D transverse phase space; (v) background level cuts are applied based on calculating the Courant-Snyder invariant for each peak (equivalent to an L_2 metric in phase space) and rejecting outlying, 'unphysical' peaks [10]; and (vi) the final values for the emittances and their uncertainties are calculated.

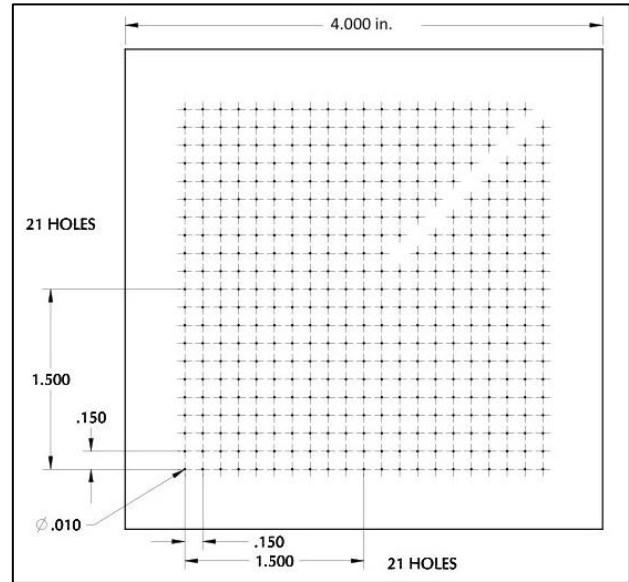


Figure 2: Pattern for the NDCX-II pepperpot mask.

The systematic measurement uncertainties, $\sigma_x^2, \sigma_{x'}^2, \sigma_y^2, \sigma_{y'}^2$, are determined from the geometry of the pepperpot mask, camera resolution, and scintillator standoff distance.

$$\sigma_x^2 = \sigma_y^2 = \frac{(\text{hole spacing})^2}{12} + \frac{(\text{resolution})^2}{12} \quad (15)$$

$$\sigma_{x'}^2 = \sigma_{y'}^2 = \frac{\left(\tan^{-1} \left[\frac{1}{\text{resolution} * \text{standoff}} \right]\right)^2}{12} \quad (16)$$

In the NDCX-II pepperpot, the systematic errors are 1.1 mm (σ_x, σ_y) and 3.5 mrad ($\sigma_{x'}, \sigma_{y'}$).

The variation in intensity is calculated for each pixel in the image region of interest (ROI). Equal numbers of images are acquired with the beam present as are background images without beam. Average values and their variances are calculated on a pixel-by-pixel basis for both the beam image and the background sets. The variance in intensity at each pixel is then determined by $\sigma_{\rho_i}^2 = \sigma_{\text{image}_i}^2 + \sigma_{\text{background}_i}^2$, where the index i labels each individual pixel. The calculation of the variances of the product terms, eqn. (2), is given in the Appendix.

Pepperpot Image Analysis

Results of the pepperpot analysis are shown in Figs. 3, 4, 5 below. The background subtracted image is shown in Fig. 3 alongside the mapping of the pixel intensity onto the transverse coordinate space (x - y). The horizontal ($x - x'$) and vertical ($y - y'$) phase spaces are shown in Fig. 4. Finally, the velocity-space distributions are shown in Fig. 5. Here the angular momentum is defined as $j_i = x_i y'_i - x'_i y_i$, where the index i labels individual beamlets in the pepperpot image.

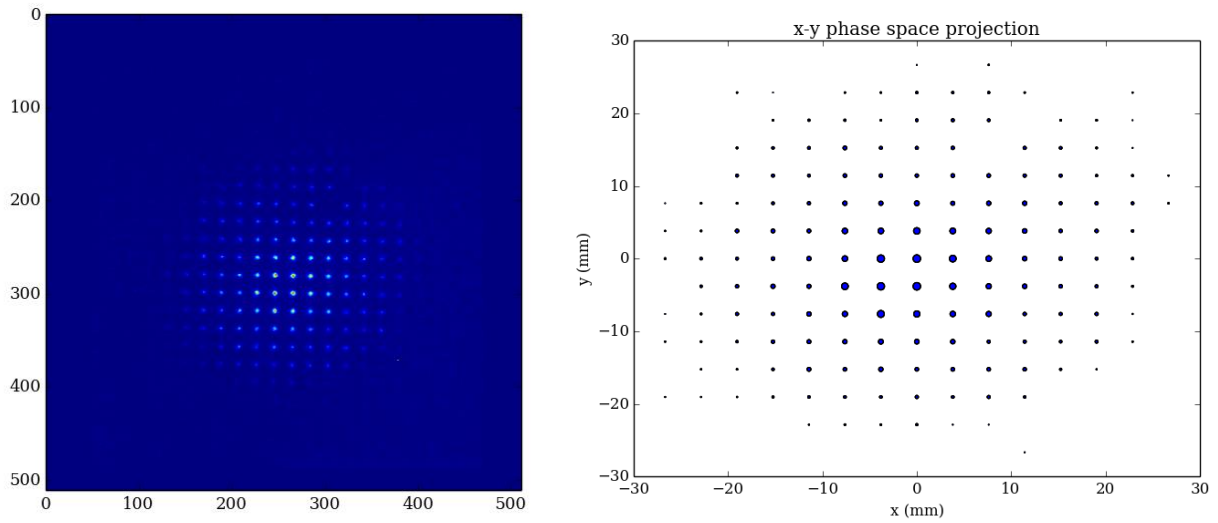


Figure 3: Pepperpot false color intensity image (left) and mapping (right).

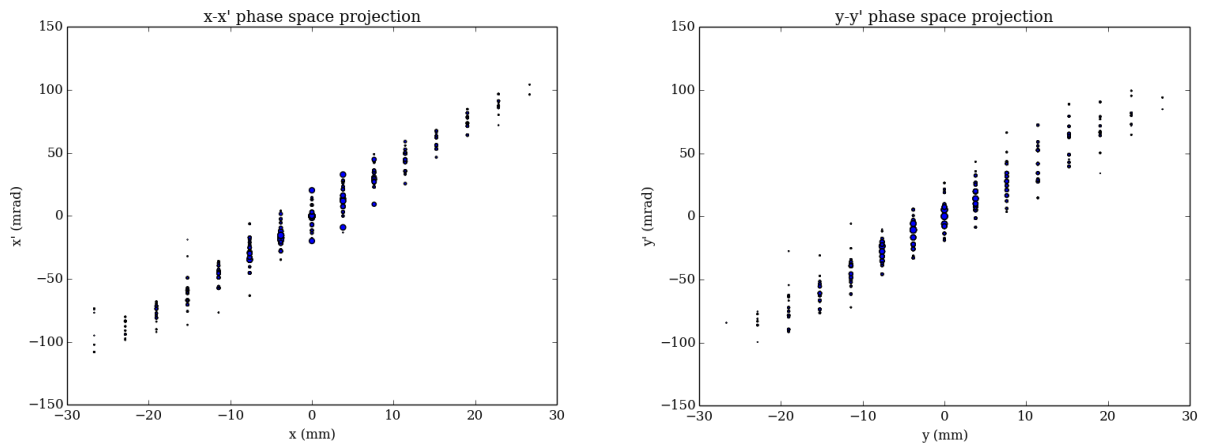


Figure 4: Cartesian phase space projections in the horizontal (left) and vertical (right) planes.

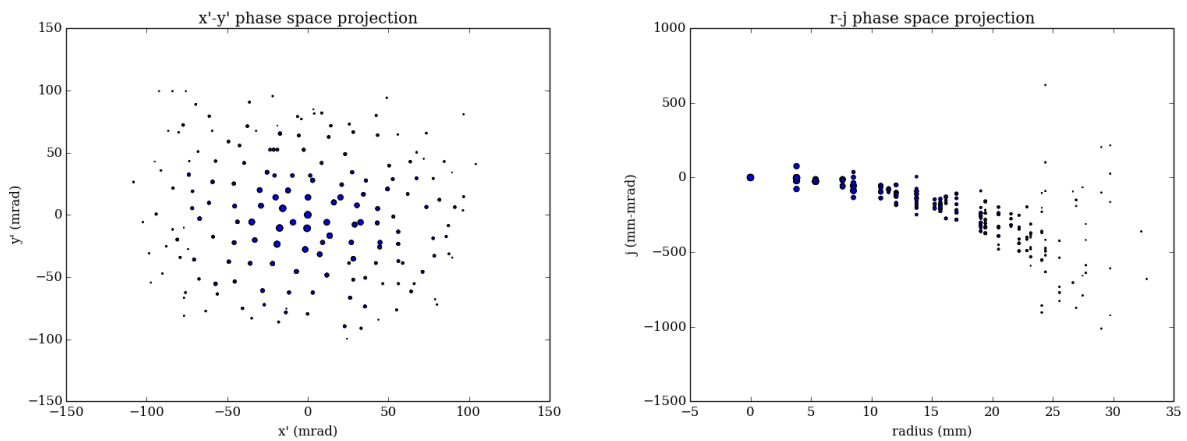


Figure 5: Velocity space (left) and angular momentum correlation (right).

Emittance Measurements

We apply the variance analysis to determine the uncertainties present in the emittance measurements as the beam focus is changed by varying the strength of the final focus magnet. The results of the scan are shown in Fig. 6. We can see that the uncertainties in the emittance measurement vary as the beam is focused - the uncertainties increase significantly as the waist moves from downstream of the pepperpot mask to upstream of the mask.

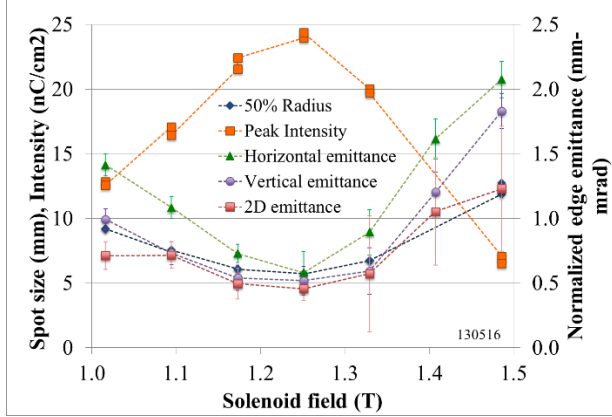


Figure 6: Variation of beam intensity, spot size, and emittances at the target plane with change in the final focus solenoid peak field.

We seek to understand the contributions of the individual measurement errors to the overall measurement uncertainty. To do so we recalculate the total uncertainties while sequentially equating all but one of the errors to zero. The results are shown in Fig. 7. We see that the relative influence of the position error increases, and that of the angle error decreases, as the beam is brought to a waist at the mask location. The opposite trend is observed as the waist moves upstream. The relative influence of the intensity error remains essentially constant for a converging beam, but increases as the waist moves farther upstream.

SUMMARY

We have performed the construction of the uncertainty in the fully correlated 4-D emittances from errors inherent in pepperpot measurements. We have demonstrated the effect of individual errors on measurements of correlated beams.

ACKNOWLEDGMENT

We would like to acknowledge the assistance of William Ghiorso in designing and fabricating the pepperpot mask used in the emittance measurements, and Wayne Greenway and Tak Katayanagi for fabricating and modifying the NDCX-II target diagnostics.

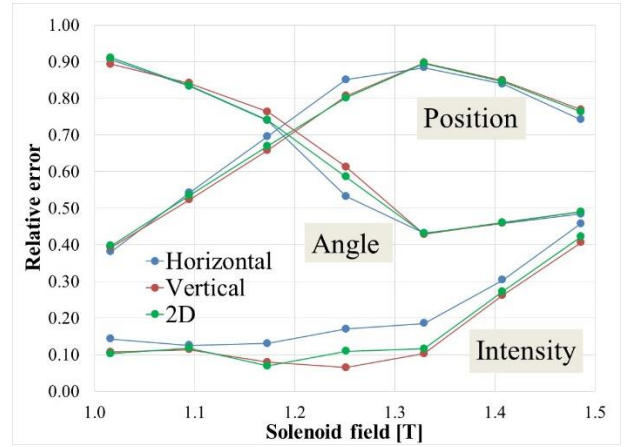


Figure 7: Contribution of the individual measurement errors to the emittance uncertainties. The total uncertainty is the quadrature sum of components.

APPENDIX: PRODUCT UNCERTAINTY

The net uncertainty in the product terms are derived.

$$\langle fg \rangle = \frac{\sum_i \rho_i f_i g_i}{\sum_i \rho_i} \quad (A1)$$

$$\sigma_{\langle fg \rangle}^2 = \sum_i \left\{ \left(\frac{\partial \langle fg \rangle}{\partial \rho_i} \right)^2 \sigma_{\rho_i}^2 + \left(\frac{\partial \langle fg \rangle}{\partial f_i} \right)^2 \sigma_{f_i}^2 + \left(\frac{\partial \langle fg \rangle}{\partial g_i} \right)^2 \sigma_{g_i}^2 \right\} \quad (A2)$$

$$\sigma_{\langle fg \rangle}^2 = \sum_i \left\{ \sigma_{\rho_i}^2 \left[\frac{f_i g_i}{\sum_k \rho_k} - \frac{\langle fg \rangle}{\left(\sum_k \rho_k \right)^2} \right]^2 + \sigma_{f_i}^2 \left[\frac{\rho_i g_i}{\sum_k \rho_k} \right]^2 + \sigma_{g_i}^2 \left[\frac{\rho_i f_i}{\sum_k \rho_k} \right]^2 \right\} \quad (A3)$$

REFERENCES

- [1] S. Jolly, *et al.*, Proceedings of DIPAC'09, WEOA03, Basel, Switzerland, (2009); <http://www.JACoW.org>
- [2] A. Burov, S. Nagaitsev, and Ya. Derbenev, *Phys. Rev. E* 66, 016503, (2002).
- [3] D.A. Edwards and L.C. Teng, *IEEE Trans. Nucl. Sci.* 20, 885, (1973).
- [4] Press, W. H.; Flannery, B. P.; Teukolsky, S. A.; and Vetterling, W. T., *Numerical Recipes in FORTRAN: The Art of Scientific Computing, 2nd ed.* Cambridge University Press, pp. 89-91, (1992).
- [5] John R. Taylor, *An Introduction to Error Analysis, 2nd ed.*, University Science Books, (1997).
- [6] A. Friedman, *et al.*, *Phys. Plasmas* 17, 056704, (2010).
- [7] W. Waldron, *et al.*, *Nucl. Instrum. Methods Phys. Res. A* 733, pp. 226-232, (2014).
- [8] S. Lidia, submitted to PRSTAB, (2014).
- [9] John C. Russ, *The Image Processing Handbook, 4th ed.*, CRC Press, (2002).
- [10] M. Stockli, R.F. Welton, R. Keller, *Rev. Sci. Instrum.* 75, 1646, (2004).